JMEPEG (2004) 13:69-77
DOI: 10.1361/10599490417524

1059-9495/$19.00

Diagnosis of Oxide Films in Cast Aluminum Alloys

Yeong-Jern Chen, Hwei-Yuan Teng, and Yuo-Tern Tsai

(Submitted 16 June 2003; in revised form 25 June 2003)

Aluminum (Al) alloy castings often contain many defects, such as micro-shrinkage, gas pores, shrinkage pores, hot tearing, and oxide film entrapment. When oxide films are entrapped in Al alloy castings, they are very difficult to identify simply by optical observation. In this study we used an auto-scanning eddy current testing method to detect oxide films entrapped in Al alloy castings. The detection signal and the measurement data were confirmed by scanning electron microscope (SEM) observation and partly backed-up by the ultrasonic-vibration method.

Keywords cast aluminum, cavitation, eddy current testing, oxide films, ultrasonic

1. Introduction

Aluminum (Al) alloy castings may contain defects such as oxide films, hot cracks, pores, and inclusion particles. These defects greatly affect the reliability and the fatigue life of the materials. When Al alloys are melted or poured, an amorphous Al_2O_3 film forms within milliseconds whenever the fresh molten Al surface is exposed to an oxygen atmosphere. This amorphous Al_2O_3 film will then crystallize if sufficient time and temperature are given. Oxide films can serve as nucleation sites for the formation of pores in cast aluminum alloys, which significantly affects the mechanical properties of the castings. Nyahumwa et al.[1] studied the effect of mold filling turbulence on the fatigue properties of cast Al alloys. They observed that a fatigue crack is initiated at the oxide film site. Therefore, the proper design of a gating system is important for reducing the entrapment of oxide films in cast Al alloys. Such entrapped oxide films are usually tiny in size and randomly distributed in the matrix of the Al alloys. In fact, the locations of entrapped oxide films depend on the quality of the melt, the gating system, with or without using filters and the complexity of the casting geometry.

Once an oxide film is entrapped in the matrix, it has been relatively difficult to identify with optical microscopic observations or to be detected by the currently available testing techniques. Huang et al.[2] have proposed an ultrasonic-vibration treatment to investigate cavitation damage to oxide films entrapped in Al-silicon (Si)-magnesium (Mg) alloys. Eroded oxide films will result in foggy marks on the polished surface that clearly indicate the existence and the extent of oxide films. Their test results were confirmed by scanning electron microscope (SEM) observation coupled with energy dispersive x-ray analyzer (EDAX) analyses. However, such testing is time consuming. In addition, when the oxide films are located in the subsurface of a specimen, it is almost impossible to identify the location or the morphology of the oxide film. Entrapped oxide films are usually very thin. This greatly reduces the capability and efficiency of radiographic non-destructive testing methods.[3] Eddy current testing is another non-destructive testing method and is based on the principles of electromagnetic induction. It has been used to identify a wide variety of physical, structural and metallurgical conditions in electrically conductive ferromagnetic and non-ferromagnetic metals. So far, eddy current technology has been successfully used to identify cracks, corrosion and major metallurgical differences in alloys.[4]

Oxide films entrapped in the Al alloy matrix are usually of a very limited thickness and/or a small opening at the interface of the Al matrix and oxide film, and also possess a specific electrical conductivity, different from that of the Al matrix. If there is a flaw or discontinuity in the material's structure, there is a phase and amplitude change on the impedance plane during eddy current testing.[5-7] This change can be observed on an oscilloscope and can be used to determine the characteristics of the defect. Maximum indication sensitivity is obtained when a crack is oriented in a direction perpendicular to the current flow; i.e., cracks lying parallel to the current path would not cause any significant interruption and may not be detected. In general, the conducting of an eddy current scan followed by a pencil probe usually generates a complicated signal and large noise, if the testing is carried out manually. The conventional eddy current testing method cannot reliably detect surface defects less than about 0.1 mm in depth because the detected signals are indistinguishable from the lift-off noise caused by probe wobble.[8] Therefore, an X-Y table, combined with an automatic scanning system, is necessary to analyze the surface defects and has been adopted in this work. Eddy current testing for oxide films, however, is not simple. Each oxide film will alter the conductivity of the aluminum alloy only a very small amount. Detecting these small changes requires stringent control of the instrument, the probe, the sample, and the measurement conditions.[4] In the present work, we propose using an eddy current inspection method to detect oxide films and defects in cast Al alloys. In addition, an ultrasonic-vibration method was also adopted to confirm the reliability of the oxide film using eddy current testing.

Yeong-Jern Chen, Hwei-Yuan Teng, and **Yuo-Tern Tsai,** De Lin Institute of Technology, Department of Mechanical Engineering, Tu-Cheng, Taiwan 236, Republic of China. Contact e-mail: jern@dlit.edu.tw.

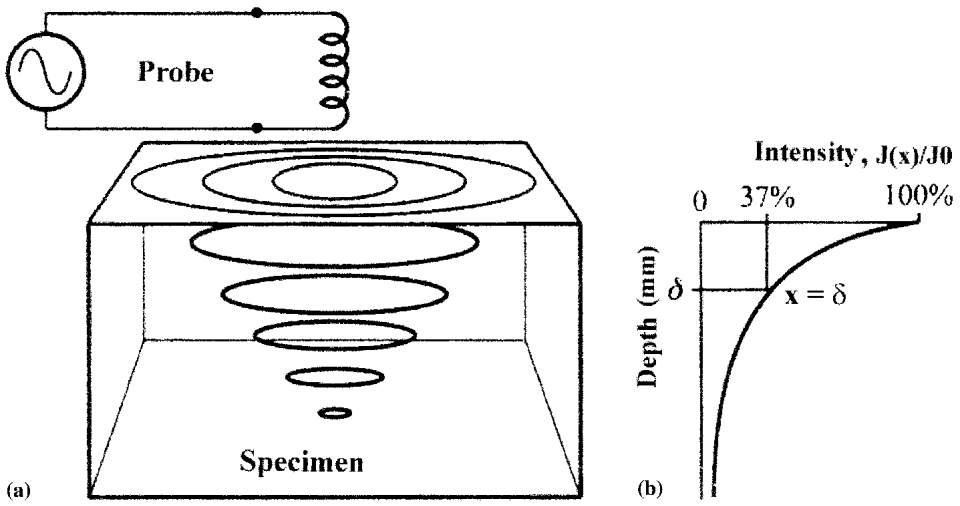

Fig. 1 Variations in eddy current density as a function of the depth below the sample's surface

2. Theoretical Background

2.1 Principles of Eddy Current Testing

Eddy current testing is one of the non-destructive testing (NDT) methods; its application is based on the law of electromagnetic induction: Faraday's law. When a coil carries an electrical current to the vicinity of conductive materials, an eddy current will be induced in the specimen. Changes in the intensity or flow of eddy currents are caused by the presence of cracks, or the existence of other phases. The thickness and shape of the specimen itself can affect the response of the eddy current. Changes on variations in spacing between the probe coil and the conductor or specimen being inspected are called lift-off. The induced eddy currents are not uniformly distributed throughout a specimen; they are usually most dense at the surface of the specimen, resulting in the so-called skin effect. Therefore, eddy current testing (ECT) is only suitable for detecting defects on the surface or the subsurface of a specimen. The eddy current density decays as a function of the depth below the surface of the tested specimen. This relation can be expressed as[9]

$$J(x)/J_0 = e^{-(x/\delta)} \sin(\omega t - x/\delta) \quad \text{(Eq 1)}$$

where $J(x)/J_0$ is the eddy-current density ratio between a depth x and the surface, δ is the standard depth of penetration (mm), and the angular frequency ω (rad/s) is given by $\omega = 2\pi/f$. The depth at which the eddy current density is reduced to a level about 37% of the density at the surface of specimen is defined as the standard depth of penetration, and is shown in Fig. 1(a) and 1(b). This depth depends on the electrical conductivity and the magnetic permeability of the material and on the frequency of the magnetizing current. The depth of penetration decreases as conductivity, permeability, or inspection frequency increase. The standard depth of penetration (δ) can be obtained from[9]

$$\delta = 50 \times \sqrt{\frac{172.41}{\sigma \mu_r f}} \quad \text{(Eq 2)}$$

where σ is the electric conductivity (%IACS), μ is the relative permeability (1 for nonmagnetic materials), and f is the inspection frequency (Hz). The standard depth of penetration as a function of the inspection frequency for several material conductivities is shown in Fig. 2. Normally, due to the skin effect, eddy current testing is restricted to depths of less than 6 mm.

A typical impedance-plane diagram is used to represent the eddy current signal, as shown in Fig. 3. The impedance Z can be expressed as

$$Z = (R^2 + X_L^2)^{1/2} \quad \text{(Eq 3)}$$

The impedance Z lies at an angle θ, called the phase angle, given by

$$\tan \theta = X_L/R. \quad \text{(Eq 4)}$$

In Eq 3, Z is the impedance (Ω), R is the alternating current (ac) resistance of the coil (Ω), and X_L is the inductive reactance of the coil (Ω), where $X_L = 2\pi f L_0$ (f is test frequency; L_0 is coil inductance). The impedance is usually plotted on an impedance-plane diagram. In the diagram, the resistance R is plotted along the X axis and the inductive reactance X_L along the Y axis. The magnitude of the impedance decreases with increasing depth of penetration, and phase angle lags behind. For a thick material, the phase angle θ can be expressed as follows[9]:

$$\theta = X/\delta \quad \text{(rad)} \quad \text{(Eq 5)}$$

$$\text{or } \theta = (X/\delta) \times 57.3^\circ \text{ (in degrees)} \quad \text{(Eq 6)}$$

Thus, for one standard depth of penetration, the phase angle is 57.3°. If an ac current is adopted, it is common to encounter a phase difference between the excitation voltage and the resultant current.

2.2 Acoustic Cavitation Damage to a Solid Surface

Ultrasonic waves are periodic sound waves, which consist of cycles of compression and expansion. Each cycle exerts a

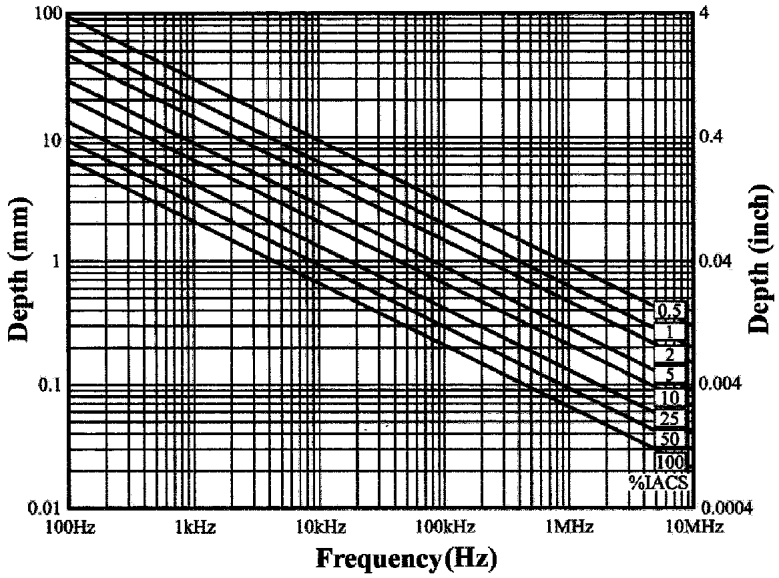

Fig. 2 Standard depths of penetration as a function of the frequencies used during eddy current inspection, for several conductivities

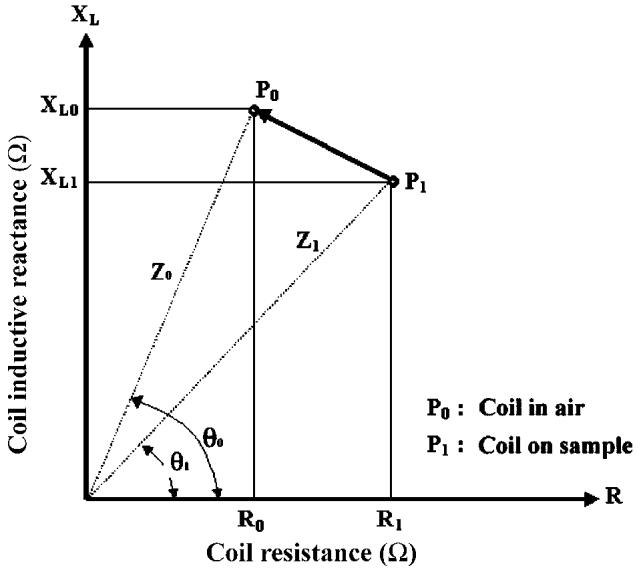

Fig. 3 Representation of the test signals on the impedance plane

positive pressure and a negative pressure, respectively. If a large negative pressure overcomes the liquid's tensile strength during an expansion cycle, a cavitation bubble may form in the liquid.[10] When a cavitation bubble nears a solid boundary, a non-spherical symmetric flow occurs, which results in the non-spherical collapse of a bubble.[11] Suslick[12] has described the asymmetric implosion of a cavitation bubble, which expels a micro-jet at high speed, which in turn produces shock waves. Chen et al.[13] stated that the micro-jet can expect to be as large as 60 μm in mean diameter; the impact velocity may vary from 30-130 m/s, and the impact pressure varies from 45 to 192 MPa. The function of this micro-jet associated with the shock waves develops in the liquid and results in mechanical damage to a solid surface, due to the great impulsive pressure, as shown in Fig. 4.[14]

3. Experimental Procedures

An inductive furnace was used to melt 25 kg of Al alloy in a SiC-graphite-clay crucible. The molten liquid was held between 953 and 1018 K (680-745 °C) and was then poured into chilled copper molds to obtain samples 10 mm thick and 50 mm in diameter. After chemical analysis, the chilled samples were again polished and a transparent acetate film about 0.01 mm in thickness was attached to the surface. Eddy current inspection was then initiated. A Hocking mini-phase (vector point mode) instrument was used to carry out the eddy current inspection. It is composed of a cathode ray tube (CRT) display associated with push-button-type, automatic zero-compensation. The test frequency was about 2 MHz, and the standard depth of penetration about 0.06 mm. An absolute shielded pencil probe, 2 mm in diameter (D_p) was used as the test probe, and the magnetic field was focused into a narrow beam below the probe. The effective diameter (D_{eff}) of the probe was about 2.24 mm ($D_{eff} = D_p + 4\delta$). This probe was fixed on an X-Y table and used to automatically scan the polished surface of the chilled sample, at a scanning speed at 2.5 mm/s. To check the detection sensibility of the ECT instrument, a standard Al block was used to calibrate the eddy current inspection signal. This standard block contained three artificial notches, 0.1 mm wide and 0.2, 0.4, and 1 mm in depth. The detection signal across these notches was recorded and used to establish the phase angle-defect depth curve. The signals for defects within the cast Al alloys were recorded, and the sites of defects on the surface of the transparent film were then marked. Finally, the transparent film was removed and the chilled samples were subjected to ultrasonic-vibration treatment.

An ultrasonic cleaner equipped with a stainless steel vessel

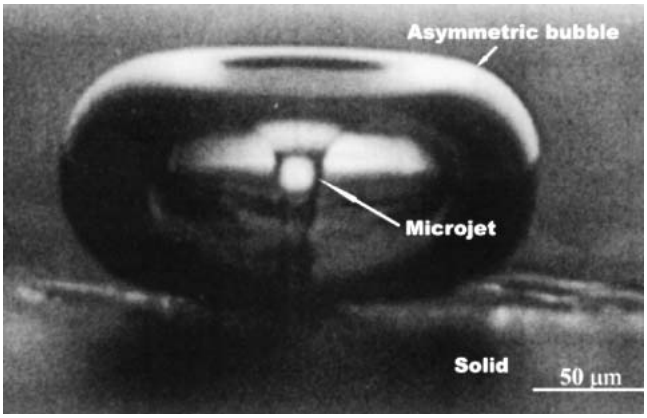

Fig. 4 Micro-jets generated from a collapsing bubble near a solid boundary

Table 1 Electric Property for Several Materials

Materials	Conductivities, IACS%	Dielectric Constant 1 kHZ, 25 °C
Al	61	…
A356	40	…
Al-7%Si	43	…
Al-13%Si	31	…
Alumina (Al_2O_3)	…	9.1
Spinel ($MgAl_2O_4$)	…	9.9
Mullite ($3Al_2O_3 \cdot 2SiO_2$)	…	8.2
Andalusite ($Al_2O_3 \cdot SiO_2$)	…	8.2

was used in this study. This vessel was filled with tap water to a volume of 500-600 ml. A polished specimen was set face up on the bottom of the vessel. A short 30 s ultrasonic-vibration treatment was carried out at a frequency of 46 kHz, with an initial ultrasound intensity of about 40 kw/m^2. Foggy marks with different morphologies, strings, spots, or clouds were gradually revealed on the shiny surface of the specimens as the treatment time increased. The morphology of the revealed marks was observed by SEM. A transparent film corresponding to the previous sites was again attached to the polished surface of the chilled samples, and then the sites of the foggy marks compared with the oxide film locations marked on the transparent film. Finally, the reliability of the oxide film was diagnosed, using eddy current testing, and verified with the ultrasonic-vibration treatment method.

4. Results and Discussion

4.1 Identifying the Testing Sensitivity of the Eddy Current Inspection

Two standard metal blocks were supplied with high (100% International Annealed Copper Standard; IACS) and low levels of conductivity (9.5% IACS). The electric properties of several materials are shown in Table 1. In general, a discontinuity standard should ideally duplicate the test situation in terms of the material type and the geometry of the samples. Artificial discontinuities may be machined into a duplicate of the test

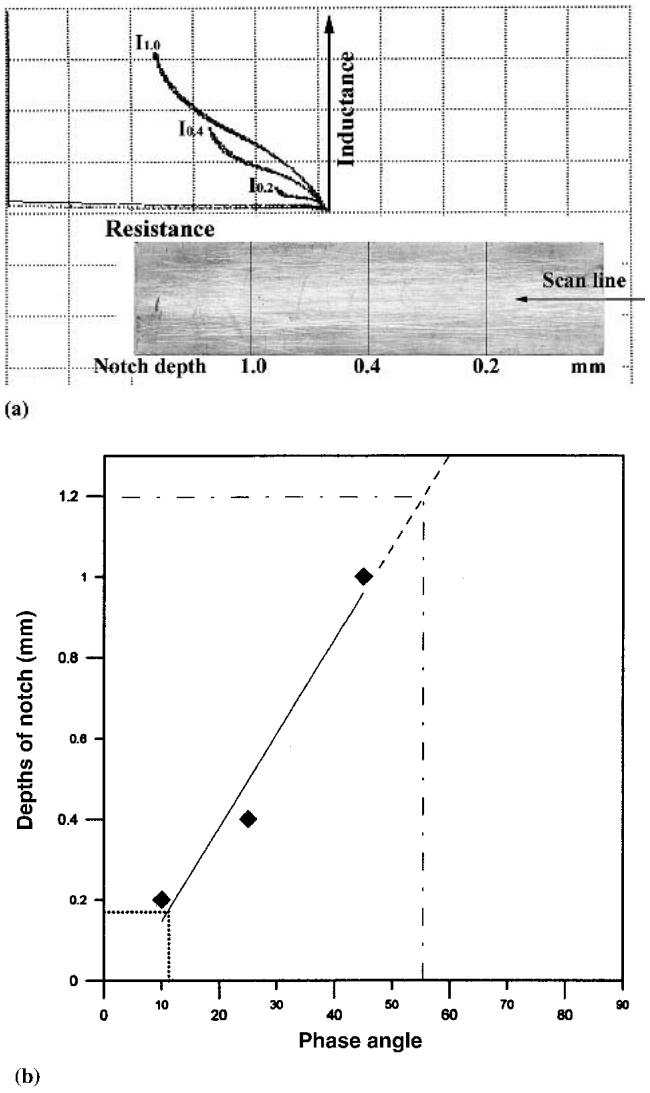

Fig. 5 Standard reference discontinuities detected via eddy current testing: **(a)** detected signals and **(b)** defect depth-phase angle curve

specimen configuration. In the present work, a standard Al reference block containing three linear notches was used to simulate the specimen. The detection signals and the defect depth-phase angle curves are shown in Fig. 5(a) and 5(b), respectively.

4.2 Clarifying Defect Types by Eddy Current Testing

Several defects, such as micro-shrinkage, hot tears, gas pores, shrinkage pores, and oxide film entrapments are often found in cast Al alloys. Of these defects, the size of oxide film entrapment is far smaller than the other defects; therefore, the detected oxide film signal is usually ignored in eddy current testing, due to the weak response. Consequently, prior to diagnosing the oxide films, the signals of the other defects must be clearly identified via eddy current testing.

Tearing or hot cracking occurs during the solidification process, when there is the greatest amount of shrinkage in the

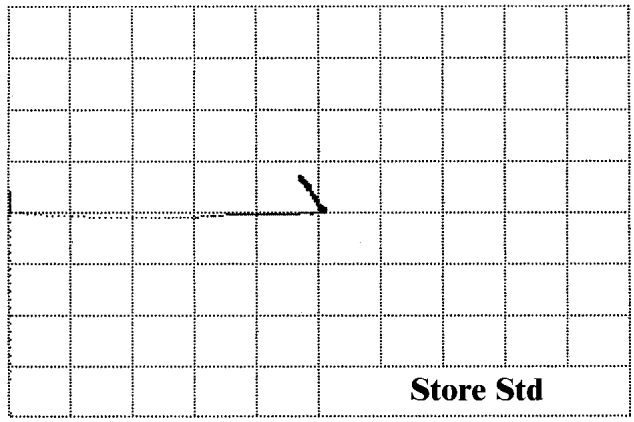

(a)

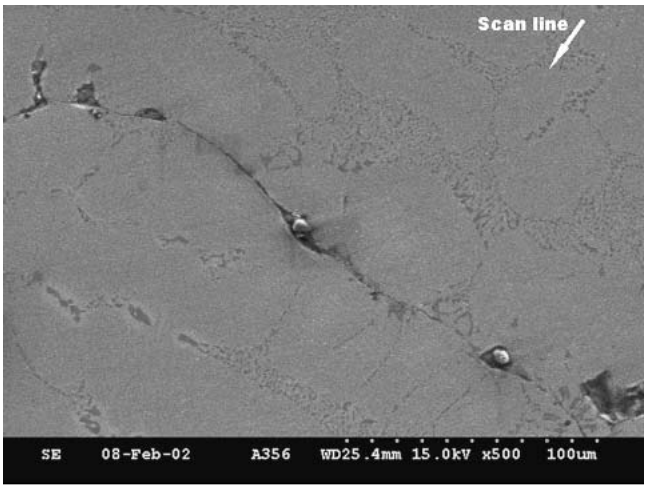

(b)

Fig. 6 Eddy current inspection of entrapped oxide film along with micro-cracks in the A356 alloy: **(a)** detected signal and **(b)** SEM observations of the micro-crack

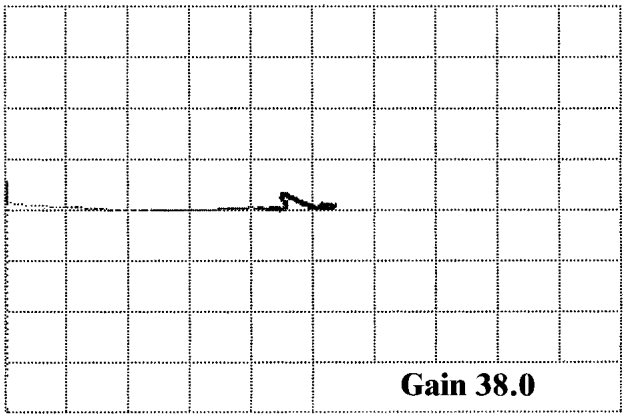

(a)

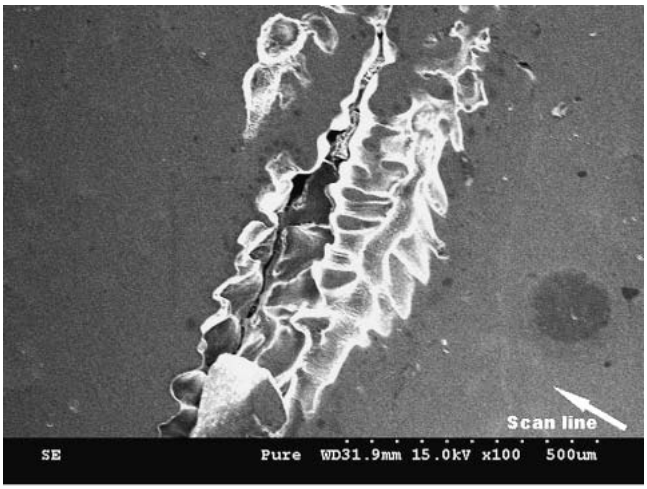

(b)

Fig. 7 Eddy current inspection of micro-shrinkage in cast aluminum: **(a)** detected signal and **(b)** SEM observations of the micro-shrinkage

casting process. Figure 6(b) shows an oxide film along with a micro-crack in the matrix of A356 Al alloy, where a small opening induced by the oxide film has become detached from the Al matrix. When a probe scans the polished surface of the chilled sample, the eddy current flow will be impeded by the presence of the micro-crack. This change in eddy current flow causes a change in the impedance of the test circuit, which can be observed on an oscilloscope, as shown in Fig. 6(a). The depth of the micro-crack corresponding to the curve of the defects depth-phase angle is about 1.2 mm, as shown in Fig. 5(b). Figure 7(b) shows some micro-shrinkage in the cast Al along with a micro-crack. Apparently, the detected signal is close to the crack's eddy current testing response (Fig. 7a), and the depth of the micro-crack as estimated from the curve of defect depth-phase angle is about 0.18 mm. It is important to differentiate between gas pores and shrinkage pores during eddy current testing. The former is due to the presence of trapped gas, and such defects are usually rounded upon metallographic examination. The latter is due to inadequate feed melting during final solidification. A gas pore about 200 μm in diameter, in the cast A356 Al alloy sample is shown in Fig. 8(b); its ECT response is shown in Fig. 8(a). A probe scanning a small area where a gas hole exists, as a result of a decrease in conductivity in Al matrix, will show a vector point in continuous motion upward on the impedance plane. When the probe has passed the area covering the gas hole, the vector point returns to the original point on the impedance plane. A number of additional compounds can be considered as inclusions in cast Al alloys. Their effect on the mechanical properties of the specimen leads to increased stress concentration. In most cases, the inclusion size is far smaller than the probe size, and cracks between inclusions and the surrounding matrix seldom appear. Consequently, eddy current testing is difficult to apply for inclusion inspection.

4.3 ECT Response on Oxide Films

As mentioned earlier, signal changes for several types of defects have been detected. Consequently, we find that the eddy current testing method allows the inspection of oxide films. Al and its alloys oxidize readily in both their solid and molten states, providing a continuous self-limiting film.[15]

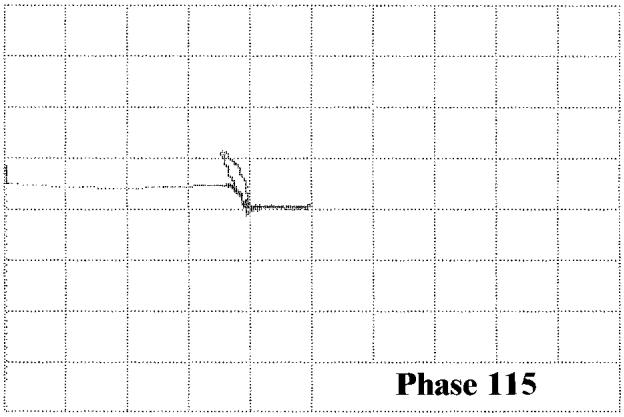

(a)

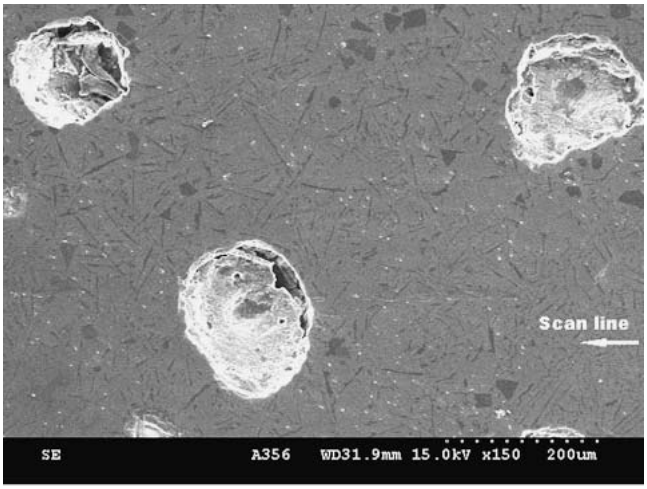

(b)

Fig. 8 Eddy current inspection of gas holes in the A356 alloy: **(a)** detected signal and **(b)** SEM observations of the gas hole

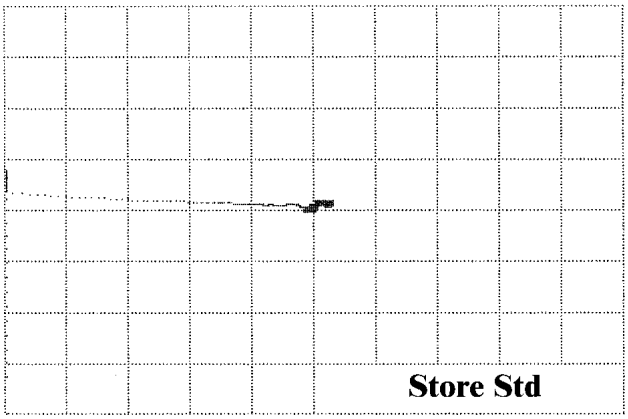

(a)

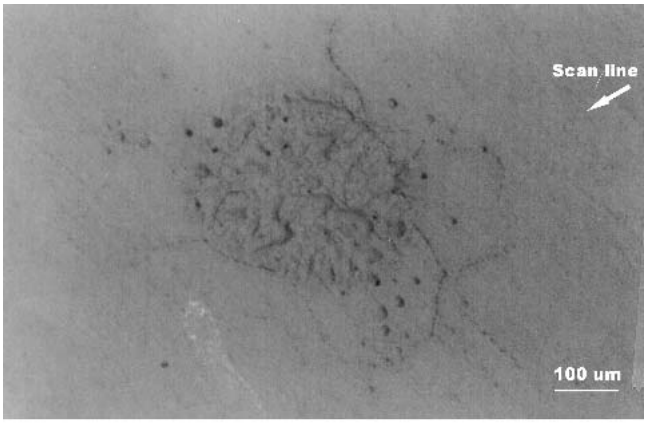

(b)

Fig. 9 Eddy current inspection of oxide films in cast aluminum: **(a)** detected signal and **(b)** optical observations of the oxide film

Al oxide (alumina, Al_2O_3) is polymorphic, but at the temperature of molten metal, the most commonly encountered forms of oxide film are crystalline, with a variety of types, depending on the exposure, temperature, and time. For Al-Si alloys, it is common to detect the existence of different oxide phases (Al, Si, and O) in the oxide film, such as mullite ($3Al_2O_3 \cdot 2SiO_2$) or andalusite ($Al_2O_3 \cdot SiO_2$).[16] The A356 Al alloys contain Mg, which oxidizes more readily and more continuously as a function of time and temperature. Mg oxide most frequently occurs in the form of micro-size particles. At a higher holding temperature (>745 °C), complex Al-Mg oxide films (Spinel, $MgAl_2O_4$) are formed, with a potential for rapid growth.[15] As a result, the oxide film provides non-uniform specific dielectric properties in cast Al alloys; thus they can be detected by eddy current testing. A brittle oxide film entrapped in cast Al alloys has different thermal expansion coefficients, which will induce a small opening during rapid cooling (possibly producing a micro-crack). In this situation, inspections of the oxide films using the ECT method are more reliable. Eskin[17] indicated that oxide films could create pores, making it very difficult to differentiate between the detected signals of oxide films and pores. Oxide films entrapped in cast aluminum will lead to the reduction of conductivity in the Al matrix. When the oxide film coalesces within the cast Al matrix, but no cracks occur at the interface (Fig. 9b); this may lead to the vector pointing slightly upward on the impedance plane, revealing a weak ECT signal, as is shown in Fig. 9(a).

4.4 Oxide Films and Defects Response on the Impedance Plane

Figures 6-9 show individual changes on the impedance plane for various types of defects, such as oxide films, shrinkage, cracks (or oxide film openings), and pores. Figure 10 illustrates the relationships (position and phase) of different defects on the impedance plane. The figure data may be used to determine how each defect responds on the impedance plane and what results are to be expected before any tests are performed. The probe-to-sample spacing is referred to as the lift-off, and the different Al alloy conductivities can be seen in the conductivity loci on the impedance plane. The polished surface of the chilled aluminum samples is detected using an absolute ECT probe. The signals detected from different defects, such as oxide films, cracks (or oxide film openings), and pores are shown on the impedance plane. Pure Al, Al-Si, and A356 al-

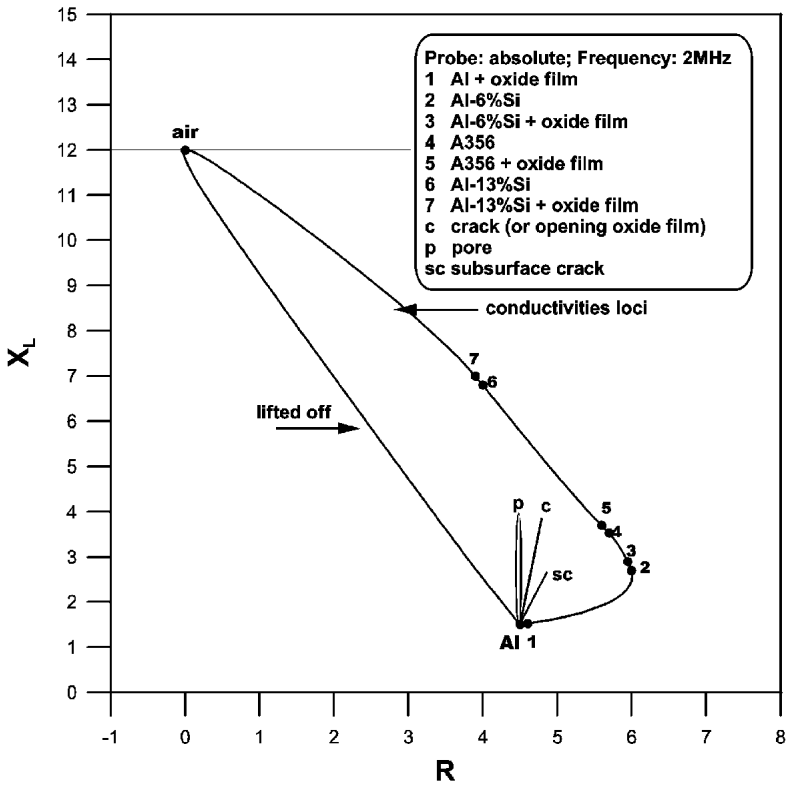

Fig. 10 Impedance changes in relation to different defects on the impedance plane

loys will respond to different conductivities on the impedance plane. Oxide films that show a small variation in the conductivity loci compared with Al matrix, which is shown in Fig. 10. Figure 11 shows that, for the A356 aluminum alloys, the scatter diagram of the defect for the response the impedance and phase angle will change on the impedance plane. Oxide films compared with other types of defects show a small impedance and phase angle.

4.5 Comparison of Different Methods of Diagnosing Oxide Films in Aluminum Alloys

If the probe is in poor contact with the sample, the signal noise will have an effect on the oxide film inspection. Consequently, we used an automatic scanning device to inspect the oxide films entrapped in cast Al alloys that had an absolute pencil probe with 3 mm in space, for line scanning along the X and Y directions on the polished specimen surface. Each signal was recorded on the impedance plane, and the sites of any defects were marked on the transparent film attached to the polished surface the sample, as shown in Fig. 12(a). The transparent film was then removed and the chilled sample subjected to ultrasonic-vibration treatment. The acoustic impedance is the product of the density of the object and the velocity of the ultrasound. The acoustic impedances of water, Al and Al_2O_3 are 1.48×10^6, 17.06×10^6, and 40.85×10^6 (kg m/s m^2), respectively.[18] When cavitation bubbles exist near an oxide film site, they can undergo violent oscillation under the effect of high acoustic impedance. The collapse of cavitation bubbles near the specimen's surface generates very intense of micro-jet

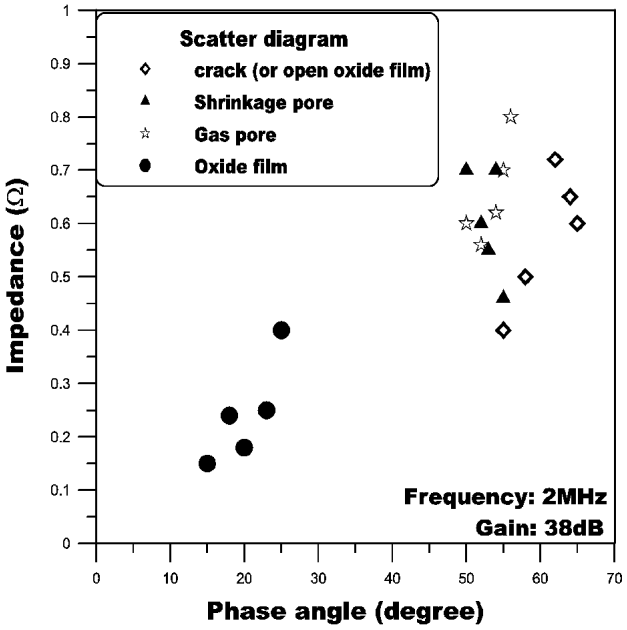

Fig. 11 Scatter diagram of the detected signal of different defects in the A356 aluminum alloy

impacts and shock waves that act on the oxide film. Finally, if the oxide film is subjected to high impulsive pressure, it can rupture and became detached from the aluminum matrix. These damaged areas appear as foggy marks, due to there being uni-

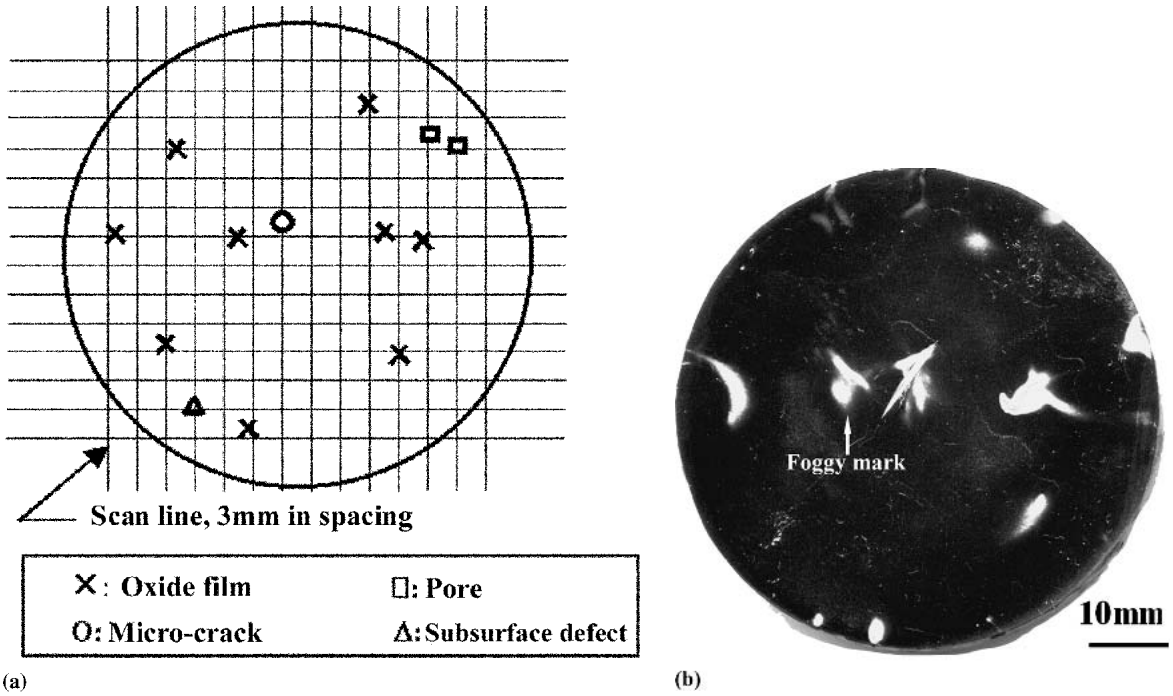

Fig. 12 Correlation of marked oxide films using different techniques: **(a)** eddy current testing and **(b)** ultrasonic-vibration treated for 1800 s

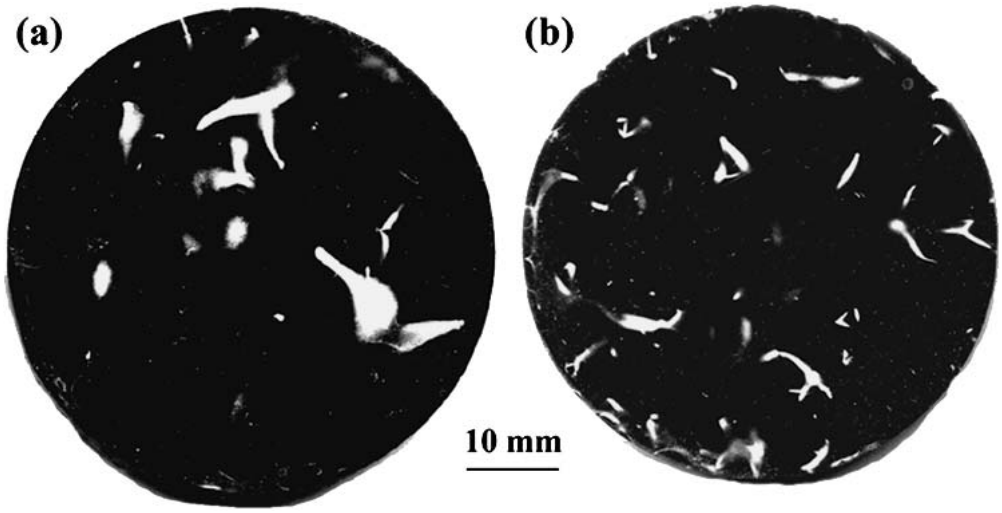

Fig. 13 Visual observations of the polished surfaces of chilled samples of **(a)** Al-7%Si alloy and **(b)** Al-13%Si alloy; ultrasonic-vibration treated for1800 s.

form light reflection at those locations. For the chilled pure Al sample after a short 1800 s ultrasonic-vibration treatment, the foggy marks on the polished surface were mostly long strips, as shown in Fig. 12(b). For Al-Si alloys, the increasing silicon content reduced the size of the foggy marks but increased the shiny spots or lumps, as shown in Fig. 13(a) and 13(b). For pure Al, the oxide films were mainly of alumina. The fractured surface (foggy marks) demonstrated mostly detached equiaxed grains of alumina, as shown in Fig. 14(a). For Al-13%Si, the fracture surfaces were mostly detached plate-like grains (Fig. 14b). Huang et al.[2] have demonstrated that these types of foggy marks exactly correspond to oxide films analyzed using an electron x-ray probe micro-analyzer (EPMA) and a scanning electron microscope SEM equipped with EDAX. After ultrasonic-vibration treatment, a transparent film according to the original position was attached to the polished surface of the chilled sample once again. Five-chilled samples were observed and analyzed, the oxide films locations marked using eddy current testing, and ultrasonic-vibration treatment showed a correlation of about 65%. It is very possible that some subsurface oxide films could not show visible damage marks after ultrasonic-vibration treatment. For the case of oxide film co-

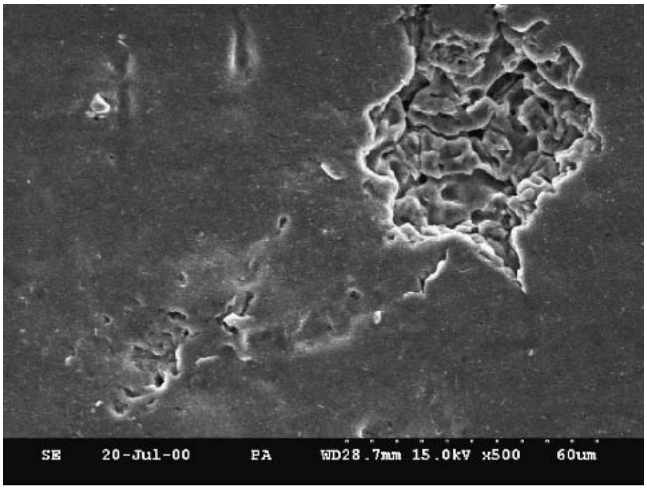

(a)

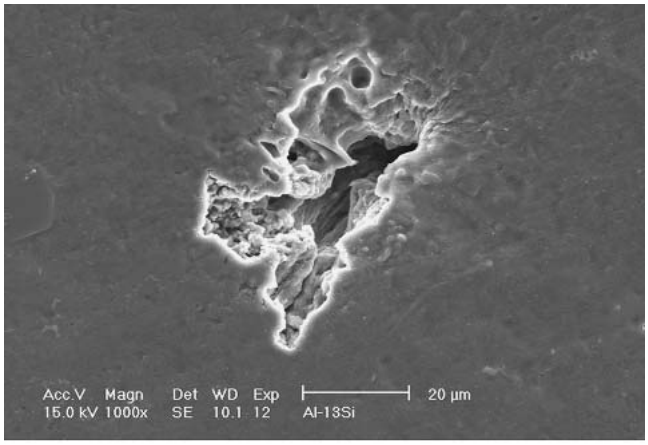

(b)

Fig. 14 The fractured surfaces of different Al alloys after ultrasonic-vibration treated at 46kHz for 15 s in 500 ml tap water: **(a)** pure Al and **(b)** Al-13%Si alloy

alescing in the aluminum matrix, a detected oxide film signal is caused by a reduction of conductivity in the specimen, as shown in Fig. 10. Since eddy current testing the oxide film produces a weak signal, all dubious signals need to be carefully identified during the eddy current testing.

5. Conclusions

Al alloy castings may contain certain defects, such as oxide films, hot cracks, micro-shrinkages, gas pores, shrinkage pores, and inclusions; these defects greatly affect the reliability of the materials. Cracks and pores should clearly produce signal changes during eddy current testing, but inclusions showed almost no response using the ECT method. Because oxide films are very thin and randomly distributed in the Al alloy matrix, the inspection of oxide films is a difficult problem. Eddy current testing is a non-destructive testing method that is based on the principles of electromagnetic induction. Oxide films have a high dielectric conductivity, with a small opening between the film and the matrix; therefore, eddy current testing can be used to identify the oxide films. ECT vibrational probe scanning produces large noise; therefore, an X-Y table can be used in association with the automatic scanning system for the inspection of oxide films. After an ultrasonic-vibration treatment, oxide films become detached from the Al matrix due to the action of cavitation damage. The damaged area can be observed optically as foggy marks. Increasing the silicon content increases the plate-like and decreases the equiaxed-type of surface fractures. The correlation of the foggy marks and the inspected oxide films was about 65%. It is very possible that some subsurface oxide films did not form foggy marks during ultrasonic-vibration treatment.

References

1. C. Nyahumwa, N.R. Green, and J. Campbell: "Effect of Mold Filling Turbulence on Fatigue Properties of Cast Aluminum Alloys," *AFS Trans.,* 1998, *106,* pp. 215-24.
2. L.W. Huang, W.J. Shu, and T.S. Shih: "Diagnosis and Analysis of Oxide Film in Al-Si-Mg Alloys," *AFS Trans.,* 2000, *108,* pp. 547-60.
3. A.Ya. Teterko, V.N. Uchanin, B.M. Rybakov, and L.N. Emelyanova: "Using Eddy Current Devices for Detecting Oxide Films in Welded Joints in Components Made of Aluminum Alloys," *Tech. Diag. Nondestruct. Testing,* 1989, *1*(2), pp. 118-19.
4. H. Chang, F.C. Schoening, and J.A. Soules: "Eddy Current Offers a Powerful Tool for Investigating Residual Stress and Other Metallurgical Properties," *Mater. Eval.,* 1999, *57*(12), pp. 1257-60.
5. X.E. Grps, K. Ogi, and K. Takahashi: "Eddy Current, Ultrasonic C-Scan and Scanning Acoustic Microscopy Testing of Delaminated Quasi-Isotropic CFRP Materials: A Case Study," *J. Reinf. Plast. Compos.,* 1998, *17*(5), pp. 389-405.
6. D.J. Hagemaier: "Eddy Current Impedance Plane Analysis," *Mater. Eval.,* 1984, *42*(7), pp. 1035-40.
7. D.J. Hagemaier: "Application of Eddy Current Impedance Plane Testing," *Mater. Eval.,* 1983, *41*(2), pp. 211-18.
8. S.R. Lampman and T.B. Zorc: "Nondestructive Evaluation and Quality Control" in *Metals Handbook,* 10th ed., ASM, Metals Park, OH, 1988, p. 187.
9. D.E. Bray and R.K. Stanley: "Fundamental Eddy Current Concepts" in *Nondestructive Evaluation,* McGraw-Hill, New York, 1993, p. 532.
10. E.A. Neppiras: "Acoustic Cavitation: An Introduction," *Ultrasonics,* 1984, *22*(1), pp. 25-28.
11. Y. Tomita and A. Shima: "Mechanisms of Impulsive Pressure Generation and Damage Pit Formation by Bubble Collapse," *J. Fluid Mech.,* 1986, *169,* pp. 535-64.
12. S. Suslick: "The Chemical Effects of Ultrasound," *Scientific American,* 1989, *80,* pp. 80-86.
13. Y.J. Chen and T.S. Shih: "Damage Pattern and Strain Energy Produced from Micro-Jet Impact," *J. CSME,* 2002, *23*(1), pp. 55-67.
14. L.A. Crum: "Comments on the Evolving Field of Sonochemistry by a Cavitation Physicist," *Ultrason. Sonochem.,* 1995, *2*(2), pp. 147-52.
15. E.L. Rooy: "Casting, Aluminum and Aluminum Alloys" in *Metals Handbook,* 10th ed., ASM, Metals Park, OH, 1988, p. 748.
16. Y.J. Chen, L.W. Huang, and T.S. Shih: "Marking Oxide Films on the Section of Al-XSi Alloys by Ultrasonic-Vibration Treatment," *Mater. Trans.*, 2003, *44*(6), pp. 1-8.
17. G.I. Eskin: "Cavitation Mechanism of Ultrasonic Melt Degassing," *Ultrason. Sonochem.,* 1995, *2*(2), pp. 167-73.
18. A.S. Birks and R.E. Green, Jr.: "Ultrasonic Testing" in *Nondestructive Testing Handbook,* American Society of Nondestructive Testing, Columbus, OH, 1991, pp. 838-41.